Atmos. Meas. Tech. Discuss., 3, 4285–4311, 2010
www.atmos-meas-tech-discuss.net/3/4285/2010/
doi:10.5194/amtd-3-4285-2010

Atmospheric
Measurement
Techniques
Discussions

MS/MS studies on the selective on-line detection of sesquiterpenes using a flowing afterglow-tandem mass spectrometer

J. Rimetz-Planchon[1], **F. Dhooghe**[1,2], **N. Schoon**[1], **F. Vanhaecke**[2], and **C. Amelynck**[1]

[1]Belgian Institute for Space Aeronomy, Ringlaan 3, 1180 Brussels, Belgium
[2]Dept. of Analytical Chemistry, Ghent University, Krijgslaan 281, S12, 9000 Ghent, Belgium

Received: 3 September 2010 – Accepted: 20 September 2010 – Published: 5 October 2010

Correspondence to: C. Amelynck (crist.amelynck@aeronomie.be)

Published by Copernicus Publications on behalf of the European Geosciences Union.

Abstract

A Flowing Afterglow-Tandem Mass Spectrometer (FA-TMS) was used to investigate the feasibility of selective on-line detection of a series of seven sesquiterpenes (SQTs). These SQTs were chemically ionized by either H_3O^+ or NO^+ reagent ions in the FA, resulting among others in protonated SQT and SQT molecular ions, respectively. These and other Chemical Ionization (CI) product ions were subsequently subjected to dissociation by collisions with Ar atoms in the collision cell of the tandem mass spectrometer. The fragmentation spectra show similarities with mass spectra obtained for these compounds with other instruments such as a Proton Transfer Reaction-Linear Ion Trap (PTR-LIT), a Proton Transfer Reaction-Mass Spectrometer (PTR-MS), a Triple Quadrupole-Mass Spectrometer (QqQ-MS) and a Selected Ion Flow Tube-Mass Spectrometer (SIFT-MS). Fragmentation of protonated SQT is characterized by fragment ions at the same masses but with different intensities for the individual SQT. Distinction of SQTs is based on well-chosen intensity ratios and collision energies. The fragmentation patterns of SQT molecular ions show specific fragment ion tracers at *m/z* 119, *m/z* 162, *m/z* 137 and *m/z* 131 for α-cedrene, δ-neoclovene, isolongifolene and α-humulene, respectively. Consequently, chemical ionization of SQT by NO^+, followed by MS/MS of SQT^+ seems to open a way for selective quantification of SQTs in mixtures.

1 Introduction

Sesquiterpenes (SQTs) ($C_{15}H_{24}$) are Biogenic Volatile Organic Compounds (BVOCs) composed of three isoprene units. They are biosynthesized by plants (Kesselmeier and Staudt, 1999; Loreto and Schnitzler, 2010) to attract flower pollinators (Pichersky and Gershenzon, 2002) and to cope with environmental stress conditions (Paré and Tumlinson, 1997, 1999). SQT emissions are globally lower than those of isoprene and monoterpenes (Kesselmeier and Staudt, 1999) and the emission rates depend on the vegetation species and biotic (e.g. phenological state of the plant, infestation, ...) and abiotic (e.g. temperature and light) factors (Duhl et al., 2008; Holopainen and Gerhenzon, 2010; Loreto and Schnitzler, 2010).

The generally high reactivity (especially towards ozone) and the low vapor pressure make SQTs important actors in atmospheric chemistry and Secondary Organic Aerosol (SOA) formation. The atmospheric lifetime of SQTs against ozonolysis is typically a few minutes. A notable exception is longifolene, the lifetime of which is of the order of several days (Canosa-Mas et al., 1999; Atkinson and Arey, 2003). Experimentally determined SOA yields from the gas-particle partitioning of SQT oxidation products vary from about 30 to 85%, depending on the SQT studied and the type of oxidant (Bonn and Moortgat, 2003; Lee et al., 2006a,b). Because of the different chemistry of individual SQT, it is necessary to measure the SQT isomers independently in order to better understand the individual impact of each SQT on atmospheric processes and air quality (i.e. tropospheric ozone and SOA formation), carbon sequestration, and global change (Duhl et al., 2008; Peñuelas and Staudt, 2010).

Because of their reactive nature and their low volatility, the accurate measurement of SQTs is not straightforward. Special care needs to be taken to avoid sampling and preconcentration artifacts when using conventional techniques based on gas chromatography (Helmig and Arey, 1992; Helmig et al., 2003). Due to the high sensitivity of Chemical Ionization Mass Spectrometry (CIMS) techniques, sampling problems are eliminated since the analysis can be carried out on-line without any need for preconcentration. Proton Transfer Reaction Mass Spectrometry (PTR-MS), a CIMS technique which uses H_3O^+ reagent ions, was recently used for the measurement of total SQT emission rates at high sensitivity and time resolution (Ezra et al., 2004; Boy et al., 2008; Bouvier-Brown et al., 2009; Kim et al., 2009).

Despite its many interesting features, an important disadvantage of PTR-MS is its lack of selectivity (Blake et al., 2009). The most common PTR-MS instruments are quadrupole-based and only allow the separation of nominal ion masses. Even if the recent development of the high resolution Proton Transfer Reaction-Time of Flight-Mass

Spectrometer (PTR-ToF-MS) (Blake et al., 2004; Jordan et al., 2009) opens the possibility of distinguishing nominally isobaric compounds on the basis of their accurate masses, the distinction of isomers remains difficult. With such an instrument, Jordan et al. (2009) recently succeeded in measuring a few pptv of SQTs in urban air of Innsbruck (Austria) based on the signal at the exact mass-to-charge ratio *m/z* of 215.1956, which corresponds with the protonated SQT ($C_{15}H_{25}^+$), produced by the proton transfer reaction with H_3O^+ reagent ions. In order to assist with SQT identification, MS techniques allowing Collision Induced Dissociation (CID) of CI product ions (MS/MS techniques) can be envisaged. Indeed, it has been shown that the intensities of the ions resulting from fragmentation processes occurring in a drift tube depend on the energy available (ratio of the electric field to the buffer gas number density, E/N) and the type of SQT (Demarcke et al., 2009; Kim et al., 2009). Consequently, the application of MS/MS techniques for the study of fragmentation schemes obtained under controlled conditions (pressure and nature of collision gas and collision energy) can be envisaged as a possibility to distinguish SQTs. Such fragmentation experiments were already performed in a Townsend Discharge Triple Quadrupole-Mass Spectrometer (QqQ-MS) and in a Proton Transfer Reaction-Linear Ion Trap (PTR-LIT) by Müller et al. (2009) to distinguish α-humulene from farnesene. These authors succeeded in differentiating these two SQTs based on the ratios of intensities of certain CID fragment ions, $I_{m/z}$, more particularly I_{149}/I_{121} and I_{93}/I_{81}. This interesting work needs to be completed by taking into account other SQTs and a range of collision energies. A part of the present study deals with the fragmentation of CI product ions, resulting from the interaction of H_3O^+ reagent ions with seven SQTs, in a Flowing Afterglow-Tandem Mass Spectrometer (FA-TMS) at different collision energies. This instrument, previously used to investigate the feasibility of such a technique for the selective detection of five C_5 unsaturated alcohols and isoprene (Rimetz-Planchon et al., 2010), has been optimized for the study of SQTs.

Müller et al. (2009) showed that the fragmentation of protonated α-humulene and farnesene resulted in different intensities of fragment ions but not in different *m/z* values for these fragments. Furthermore, no specific SQT fragment ions were found by Selected Ion Flow Tube-Mass Spectrometry (SIFT-MS) (Dhooghe et al., 2008) or PTR-MS with H_3O^+ as reagent ion (Demarcke et al., 2009; Kim et al., 2009). A further possible improvement of MS/MS techniques in order to succeed in monitoring one SQT in a mixture of several SQTs could be the use of a different reagent ion such as NO^+. This ion species was already used as CI reagent ion to distinguish isobaric and even isomeric compounds. Soft ionization of analyte molecules by NO^+ can proceed via multiple reaction mechanisms, such as association, charge and hydride ion transfer, possibly followed by fragmentation. A large library of reaction rates and product ion distributions of the reaction of NO^+ ions with many VOCs of different chemical functionalities has been built up during the last fifteen years, mainly by Španěl and Smith in support of the detection of these compounds by SIFT-MS (Španěl et al., 1997; Španěl and Smith, 1997, 1998; Smith and Španěl, 2005). Dhooghe et al. (2008) studied the product ion distribution from the CI of SQT by NO^+ in a SIFT-MS. In addition to the main SQT molecular ion at *m/z* 204 resulting from charge transfer, the authors observed some specific SQT fragment ions.

Recently NO^+ reactant ions have also been used in medium-pressure drift tube instrumentation. Wyche et al. (2005) investigated the detection of some alkenes, aromatic hydrocarbons, alcohols, aldehydes, ketones, nitriles and esters in a drift tube reactor coupled to a reflectron time-of-flight mass spectrometer (Wyche et al., 2005; Blake et al., 2006), and Knighton et al. (2009) succeeded in detecting 1,3-butadiene by employing a commercial PTR-MS in NO^+ mode. Moreover, a highly sensitive Proton Transfer Reaction-Switchable Reagent Ion-Mass Spectrometer (PTR+SRI-MS) instrument which enables the use of H_3O^+, NO^+ and $O_2^{\bullet+}$ ions (Jordan et al., 2009) has recently become commercially available (Ionicon Analytik GmbH, Innsbruck, Austria).

Even if CI by NO^+ seems to be a good approach to distinguish SQTs, Wyche et al. (2005) stated that it cannot be used routinely in a PTR-MS instrument for detection and quantification of VOCs in mixtures. Indeed, the greater degree of fragmentation that they observed with NO^+ as reagent ions (compared to CI by H_3O^+) causes spectral

interference. The use of FA-TMS with NO^+ as CI reagent ion can possibly prevent this problem, since fragmentation is performed on a parent ion isolated from the complex matrix present in the FA. Another part of the present work is therefore dedicated to the study of the fragmentation of ions produced by the reaction with NO^+, in order to find tracer ions, which could be used for the detection and the quantification of SQTs in mixtures.

2 Materials and methods

2.1 FA-TMS

The FA-TMS consists of a home-made Flowing Afterglow reactor, which is coupled to a Tandem Mass Spectrometer, custom-designed by Extrel CMS (Pittsburgh, USA). The instrument has already been thoroughly described in a previous paper (Rimetz-Planchon et al., 2010) and will only be briefly discussed here. The reaction between a SQT and a reagent ion (NO^+ or H_3O^+) takes place in the FA. The resulting CI product ions are sampled into the TMS. The CI product ion of interest, also called parent ion, is selected by a first quadrupole and enters the octupole collision cell, which is filled with the collision gas (Ar) at a pressure of 0.11 Pa. This pressure was chosen to have a sufficiently high fragmentation yield. Depending on the collision energy in the center-of-mass frame (E_{CM}), controlled by the pole bias of the octupole, one or more fragments will be produced. The fragmentation spectrum is obtained by performing a mass scan with the second quadrupole and the ions are detected with a secondary electron multiplier, operating in pulse counting mode.

The two main adaptations of the instrument needed for the present study concern the introduction system of SQTs and the production of NO^+ in the FA. Due to the low vapor pressure and the sticky nature of SQT, a static mixture of SQT vapor in an inert gas is instable. Thus SQTs are introduced dynamically in the FA by blowing a controlled small flow of argon gas over a reservoir filled with the pure liquid SQT.

The temperature of the liquid is kept constant at 279 K by immersing the reservoir in a thermostatically controlled water bath and all stainless steel tubing between the reservoir and the flow tube is heated to avoid SQT deposition. The SQT flow that enters the reactor is regulated by varying the pressure above the reservoir by means of a needle valve located between the reservoir and the flow tube.

The reagent ions NO^+ are created upstream the flow tube by the impact of electrons emitted by a thoriated iridium filament onto $NO^\bullet$. The ionization energy of $NO^\bullet$ (9.26 eV) is lower than that of Ar (15.76 eV), the flowing afterglow buffer gas, and therefore the voltage of the counter-electrode, which determines the energy of the electrons has been lowered to favor the ionization of $NO^\bullet$.

2.2 Data acquisition

Measurements were performed with seven SQTs: aromadendrene, β-caryophyllene, α-cedrene, α-humulene, isolongifolene, longifolene and δ-neoclovene.

Mass spectra of fragment and parent ions were acquired for different E_{CM} values. The calculation of E_{CM} requires the determination of the stopping potential, obtained by retardation potential analysis (Rimetz-Planchon et al., 2010). The mean stopping potential and the spread of the parent ions are $-3.8\,\mathrm{V} \pm 0.1\,\mathrm{V}$ and $1.7\,\mathrm{V} \pm 0.1\,\mathrm{V}$ Full Width at Half Maximum (FWHM), respectively. The FWHM is higher than observed in other TMS instruments (Muntean and Armentrout, 2001), but sufficient for our purposes. For each fragment, the plot of intensity as a function of E_{CM} is called appearance curve.

The range of E_{CM} was 0.6–8 eV. For $E_{\mathrm{CM}}>8$ eV, scattering and defocusing effects became too important, as characterized by a decrease of more than 50% of the maximum collection efficiency (E_c) value (Fig. 1 and Eq. 1) and deformed peaks. For $E_{\mathrm{CM}}<0.6$ eV, the uncertainty on the intensity of fragment ions was too high to exploit fragmentation data.

The values of collection (E_c), fragmentation (E_f) and CID (E_{CID}) efficiencies for the fragmentation of each protonated SQT and SQT molecular ions were calculated as

follows (Yost et al., 1979; Thomson et al., 1995; Ibrahim et al., 2010):

$$E_c\,(\%) = 100 \times \frac{I_p + \sum_i I_{fi}}{I_{p0}} \tag{1}$$

$$E_f\,(\%) = 100 \times \frac{\sum_i I_{fi}}{I_p + \sum_i I_{fi}} \tag{2}$$

$$E_{\mathrm{CID}}(\%) = 100 \times \frac{\sum_i I_{fi}}{I_{p0}} \tag{3}$$

Where I_p is the intensity of the parent ion, I_{fi}, the intensity of the fragment ion fi, and I_{p0}, the intensity of the parent ion when no collision gas is introduced in the collision cell. E_c is influenced by scattering effects, whereas E_f represents the efficiency of producing fragment ions. E_{CID} reflects these two combined effects (Ibrahim et al., 2010). E_c, E_f and E_{CID} values are similar for the SQTs studied. An example is shown for α-cedrene (Fig. 1). Values of E_c range from about 22 to 54% and from 27 to 95% for the fragmentation of protonated SQT and SQT molecular ions, respectively. Best values are found for E_{CM} values between 1.2 and 5.4 eV. Scattering increases strongly for collision energies above about 6 eV. Values of E_f range from about 5 to 76% and from 5 to 84% for the fragmentation of protonated SQT and SQT molecular ions, respectively. Best values are found for E_{CM} values between 5 and 6 eV. Values of E_{CID} vary between 2 and 40% and 2 to 41% for the fragmentation of protonated SQT and SQT molecular ions, respectively. Best values are found for E_{CM} values around 5 eV.

In order to compare the fragmentation patterns of the different SQTs, the intensity of each fragment is expressed in percentage relative to the sum of intensities of all fragments, which is called fragmentation fraction. In what follows, the Maximum Fragmentation Fraction (MFF) refers to the maximum value found along the collision energy range.

2.3 Chemicals

Aromadendrene (97%), isolongifolene (98%), α-humulene (98%), δ-neoclovene (98%), β-caryophyllene (98.5%), longifolene (99%) and α-cedrene (99%) were purchased from Fluka. Argon (99.9997%), SF_6 (1000 ppmv in Ar) and $NO^\bullet$ (5% in He) were obtained from Air Products.

3 Results and discussion

The fragmentation of protonated SQT (*m/z* 205) and SQT molecular ions (*m/z* 204) were studied for each of the seven SQTs. The list of resulting fragment ions is presented in Table 1. The fragmentation rules are respected (de Hoffman and Stroobant, 2007) as expected: the even-electrons cations (EE^+) at *m/z* 205 do not fragment into odd-electrons cations ($OE^{\bullet+}$), also called radical cations, but only into EE^+, since the fragmentation of EE^+ into $OE^{\bullet+}$ is an endothermic and thus, improbable reaction. The $OE^{\bullet+}$ at *m/z* 204 fragment into both $OE^{\bullet+}$ and EE^+. Depending on the type of fragmentation, neutral losses under the form of molecules or radicals can occur.

3.1 Fragmentation patterns of protonated SQT (*m/z* 205)

The EE^+ fragments from the fragmentation of protonated SQT were classified into five families (A to E), which each gather fragments separated by a CH_2 unit (14 u), according to the previous classification used by Dhooghe et al. (2008) and Demarcke et al. (2009) (Table 1). Dhooghe et al. (2008) determined the product ion distributions from the reactions between H_3O^+ and the seven studied SQTs in a SIFT-MS at thermal conditions in a He buffer gas, corresponding to an estimated collision energy of 0.04 eV. Demarcke et al. (2009) studied the influence of the ratio E/N on the product ion patterns from the reactions between $H_3O^+(H_2O)_n$ (n=0 to 2) and four SQTs (α-humulene, α-cedrene, longifolene and β-caryophyllene) in a PTR-MS at estimated

collision energies ranging from 0.1 to 0.3 eV. These higher E_{CM} values (compared to the value in the SIFT-MS instrument) are due to additional translational energy of the ions caused by the presence of the drift field (Blake et al., 2009). The fact that higher collision energies are used in the TMS compared to those in SIFT-MS or PTR-MS explains why Dhooghe et al. (2008) and Demarcke et al. (2009) only observed fragment ions included in the families B and C (Table 1). Kim et al. (2009) and Ezra et al. (2004) also observed fragment ions of these two families by PTR-MS for β-caryophyllene, α-humulene and aromadendrene and for α-humulene, respectively (Table 1). Lee et al. (2006a) studied the patterns of ions produced by the reaction between H_3O^+ and four SQTs (β-caryophyllene, α-humulene, longifolene and aromadendrene) in a PTR-MS. The authors found fragment ions included in the five families (Table 1). Most of the major fragment ions (*m/z* 135, *m/z* 149, *m/z* 163, *m/z* 95, *m/z* 109 and *m/z* 123) observed in SIFT-MS (Dhooghe et al., 2008) and PTR-MS (Demarcke et al., 2009) instruments are also formed in the collision cell of the FA-TMS at collision energies below 2 eV and with fragmentation fractions of at least 6%, which shows that fragmentation patterns of SQTs are generally coherent between the three techniques. It needs to be stressed, however, that one should be cautious when comparing quantitatively branching ratios obtained by FA-TMS with those obtained by PTR-MS and SIFT-MS since mass discrimination of the former instrument is not known.

Müller et al. (2009) studied the fragmentation of the protonated α-humulene in the collision cell of a QqQ-MS instrument and in the ion trap of a PTR-LIT instrument. The authors present results for two collision cell offset voltages (U_{cc}=12 and 33 V, Fig. 2a,b) and one dipolar excitation voltage ($U_{CID,PTR\text{-}LIT}$=0.13 V, Fig. 2c) for QqQ-MS and PTR-LIT, respectively. Since these voltages were not converted in collision energies in the center-of-mass frame, we decided to choose three E_{CM} values in order to compare our results with those of Müller et al. (2009): (i) 0.68 eV is the energy for which ions at *m/z* 149 reach their maximum fragmentation fraction in the collision energy range selected (Fig. 2c); (ii) 5.1 eV is the energy for which E_{CID} (Eq. 3) is maximum (Fig. 2d); and (iii) 6.4 eV is the energy for which ions at *m/z* 81 have their maximum fragmentation fraction (Fig. 2e). Although the results were not corrected for mass discrimination, spectra obtained by PTR-LIT, QqQ-MS at 12cc and FA-TMS at 0.68 eV are remarkably similar.

3.2 Fragmentation pattern of SQT molecular ions (*m/z* 204)

The EE^+ and $OE^{\bullet+}$ fragments from the fragmentation of SQT molecular ions were classified into six (A to F) and five (a to e) families, respectively (Table 1). The detailed fragmentation patterns for the individual SQT are presented in Table 2. To our knowledge, CI of SQT by NO^+ followed by CID of the resulting $SQT^{\bullet+}$ molecular ions was never performed up to now. The only data available for comparison concern the determination of the product ion distributions of the reactions between NO^+ and the SQT in a SIFT-MS at low collision energy (Dhooghe et al., 2008) and Electron Impact (EI) spectra at high collision energy (70 eV) (NIST database). Except for the ions at *m/z* 80, *m/z* 134 and *m/z* 176 from β-caryophyllene, NO^+/SQT product ions with yields >2%, as observed by Dhooghe et al. (2008), are also major fragment ions of $SQT^{\bullet+}$ (maximum fragmentation fraction >10%) produced in the FA-TMS for $E_{CM}<2$ eV. Similarities also appear between EI and FA-TMS techniques: (i) For longifolene and isolongifolene, the major fragment ion is observed at *m/z* 161 for both EI and FA-TMS techniques, the maximum fragmentation fractions values in FA-TMS being 72% and 66% for these two respective SQTs (11–37% for the other SQTs); (ii) For δ-neoclovene, the major ion in the EI spectrum is observed at *m/z* 120. In FA-TMS, this fragment ion has a maximum fragmentation fraction of 12% for this SQT, while this fraction varies between 2 and 6% for the other SQTs; (iii) The fragment ion at *m/z* 162, which is characteristic for the fragmentation pattern of ionized δ-neoclovene in the FA-TMS instrument, represents 62% of the major peak in the EI spectrum (at *m/z* 120), whereas this fraction is only between 2 and 24% for the other SQTs. In general, however, it can be stated that CID of $SQT^{\bullet+}$ in the FA-TMS results in much less fragmentation than impact of 70 eV electrons onto SQTs.

3.3 Fragmentation of other CI fragment ions

CID of product ions other than those at *m/z* 204 and *m/z* 205 formed in the FA with a sufficiently high contribution to the reactant ion/SQT product ion distribution was also investigated, as this may result in additional information or understanding of fragmentation patterns of SQT molecular ions and protonated SQT.

The CI fragment ions at *m/z* 149 (for α-humulene, aromadendrene, β-caryophyllene, δ-neoclovene and longifolene), *m/z* 135 (for α-humulene, aromadendrene, β-caryophyllene, δ-neoclovene), *m/z* 121 (for α-humulene and β-caryophyllene) and *m/z* 95 (for α-humulene, aromadendrene, β-caryophyllene, δ-neoclovene and longifolene) were produced in the FA with H_3O^+ as reagent ions and were introduced in the collision cell. CI fragment ions at *m/z* 109 and 123 were not considered in our study because of an isobaric interference present in the background.

CID of CI fragment ions of fixed *m/z* ratio do not result in specific fragment ion *m/z* values for the SQT studied. Identical CID fragmentation patterns were found, albeit with different fragment ion intensities for the different SQT species. Therefore, the fragmentation study of CI fragment ions does not really provide supplementary information for the selective detection of SQTs. With the exception of fragment ions at *m/z* 39, 53, 80, 89 and 120, all fragment ions (with a maximum fragmentation fraction >5%) resulting from the fragmentation of CI fragment ions are also produced from the fragmentation of protonated SQT (*m/z* 29, 41, 43, 55, 67, 69, 77, 79, 81, 91, 93, 105, 107, 119 and 121). It can be remarked that ions at *m/z* 89 are not included in the six families (Table 1) and that ions at *m/z* 80 and 120 are formed, despite the fact that it is expected to be thermodynamically improbable ($EE^+ \rightarrow OE^{\bullet+}$).

The CI fragment ions at *m/z* 147 (α-humulene), *m/z* 148 (β-caryophyllene), *m/z* 161 (β-caryophyllene), *m/z* 162 (δ-neoclovene), *m/z* 176 (β-caryophyllene) and *m/z* 189 (β-caryophyllene) were produced in the FA with NO^+ as reagent ions and were subjected to fragmentation in the collision cell of the FA-TMS. The fragmentation patterns of ions at *m/z* 147 (α-humulene) and *m/z* 162 (δ-neoclovene) as a function of the collision energy are presented in Fig. 3a and b, respectively. These examples have been chosen because the fragmentation of these two ions produces only a limited number of fragment ions, implying clear appearance curves. The ions at *m/z* 147 mainly fragment into ions at *m/z* 105 (maximum fragmentation fraction=98% at about 2 eV). Other fragment ions appear at higher collision energies (Fig. 3a). The link between the ions at *m/z* 147 and *m/z* 105 may explain why ions at *m/z* 105 are observed at a higher maximum fragmentation fraction for the fragmentation of the α-humulene molecular ion (40%, Table 2) than for the other SQTs (<14%, Table 2). The fragmentation of ions at *m/z* 162 (δ-neoclovene) produces fragment ions at *m/z* 147 and 106 following a bell-shaped appearance curve characterized by a maximum intensity at about 3.5 eV (Fig. 3b). The formation of the fragment ions at *m/z* 91 and 105 requires more energy since their maximum intensity is reached for collision energies >6 eV. The fragmentation of NO^+ CI fragment ions from β-caryophyllene produces lots of ions with maximum fragmentation fractions below 38%. The fragmentation patterns are detailed in Table 3.

The CI product ions at *m/z* 234 $(C_{15}H_{24}{\cdot}NO)^+$, resulting from the association reaction between NO^+ and longifolene in the FA, as it was already observed in SIFT-MS experiments (Dhooghe et al., 2008), were sufficiently stable to be introduced in the collision cell of the TMS for fragmentation by collision with Ar. At very low collision energy (close to 0 eV), the fragmentation of the adduct produces ions at *m/z* 204 ($C_{15}H_{24}^{\bullet+}$). The fragmentation process does not correspond to the reverse reaction of association taking place in the FA. This result proves that the charge, shared in the complex to assure its stability, is preferentially transferred to the sesquiterpene to form the fragment ions at *m/z* 204 after the collision process. The capability of longifolene to carry the charge can be explained by the lower ionization energy of longifolene (8.55 eV, Novak et al., 2001) compared to $NO^{\bullet}$ (9.25 eV).

3.4 Selective detection of SQTs

The fragmentation patterns of the different protonated SQTs only differ by variations in the fragment ion abundances. Selected ratios at different collision energies are

presented for the seven SQTs in Fig. 4. Müller et al. (2009) used the intensity ratios I_{149}/I_{121} and I_{93}/I_{81} for the distinction between α-humulene and farnesene. The first one can be used to distinguish all the SQTs studied in our work, whereas the second one is not appropriate to differentiate them, especially due to large uncertainties on the ratios. The ratios I_{69}/I_{123}, I_{121}/I_{123} and I_{83}/I_{135} allow to discriminate isolongifolene, α-cedrene and aromadendrene, respectively, from the other SQTs.

The fragmentation patterns of SQT molecular ions provide powerful information for the selective detection of SQTs and even their quantification. At well-chosen collision energies, some tracers can be found. A fragment ion is considered as a tracer of a specific SQT if its fragmentation fraction is at least ten times higher than for the other SQTs studied. It is the case for ions at *m/z* 119 at 0.7 eV for α-cedrene, *m/z* 162 at 0.7 eV and *m/z* 83 at 6.1 eV for δ-neoclovene, *m/z* 137 at 2.5 eV for longifolene and *m/z* 131 at 0.7 eV for α-humulene (Table 4). Through this method, an independent quantification of these four SQTs present in a mixture can be envisaged. No tracers were found for aromadendrene, isolongifolene and β-caryophyllene. However, in particular conditions where not all the studied SQTs are present in the mixture, it is possible to directly use a fragment ion to follow a particular SQT signal or to correct for the intensity of a major fragment ion. The limit of the method is sensitivity, which is different between the tracers. The sensitivity takes into account both the yield of formation of the SQT molecular ion in the FA (ranging from 77 to 99%, Table 4, Dhooghe et al., 2008) and the fragmentation fraction of the fragment ions produced in the collision cell (ranging from 3.8 to 71%). The sensitivity will be better for δ-neoclovene than for α-humulene.

4 Conclusions

Recent developments in the field of chemical ionization mass spectrometry reveal the need for selective and highly sensitive on-line techniques for detection and quantification of isobaric/isomeric BVOCs. The results of this work show that a Flowing Afterglow reactor coupled to a Tandem Mass Spectrometer (FA-TMS) can be a useful instrument to distinguish SQTs, a particular class of BVOCs of high interest to the atmospheric chemistry community.

A first part of our study focused on chemical ionization of seven SQTs using H_3O^+ reactant ions and the subsequent fragmentation of the protonated SQT in the collision cell of the tandem mass spectrometer. No specific fragment ion tracers were found for the different SQTs, but large differences in fragment ion intensity ratios were sometimes noticed between SQTs. Moreover, the measurements showed that it is often useful to look at fragment ion ratios over an extended collision energy range (0.6–8 eV in our case). Identification of the seven SQTs studied can for instance be envisaged from the ratio I_{121}/I_{149}, and the ratios I_{69}/I_{123}, I_{121}/I_{123} and I_{83}/I_{135} were found to be much larger for isolongifolene, α-cedrene and aromadendrene, respectively. However, in agreement with Müller et al. (2009), who recently applied this method in a PTR-LIT and in a QqQ-MS provided with a Townsend Discharge ion source for two SQT species, we have to conclude that on-line identification and quantification of individual SQT in a mixture containing more than one SQT by MS/MS of protonated SQT will be extremely difficult.

In a second part of the present study, the use of NO^+ reactant ions for chemical ionization of SQTs, followed by CID of the resulting $SQT^{\bullet +}$ ions was investigated. This methodology looks far more promising, as it resulted in fragment ion tracers for four out of the seven SQTs studied: α-cedrene, δ-neoclovene, longifolene and α-humulene, and this opens a way to selective on-line quantification of SQTs in more complex matrices. Of course these measurements will still have to be accompanied by a powerful off-line technique for SQTs identification, such as GC-MS, and the other SQT (not among the seven SQTs studied) will have to be introduced individually in the on-line CIMS instrument in search for tracers.

The present study has focused on selective detection of SQT isomers and not on their quantification. In its present state, the FA-TMS is not able to quantify SQTs in air at mixing ratios that are typical for field studies (some pptv). In order to drastically enhance the detection sensitivity, future work will deal with the replacement of the FA

reactor by a drift tube reactor coupled to a hollow cathode discharge ion source for the production of large concentrations of NO^+ reactant ions.

Acknowledgement. The authors gratefully acknowledge the financial support of the Belgian Federal Science Policy (research projects #MO/35/022 and #MO/35/026) and of the Institute for the Promotion of Innovation through Science and Technology in Flanders (IWT-Vlaanderen). They also thank David Smith for providing interesting comments on some ion chemistry related aspects of this work.

References

Atkinson, R. and Arey, J.: Gas-phase tropospheric chemistry of biogenic volatile organic compounds: a review, Atmos. Environ., 37, 197–219, 2003.

Blake, R. S., Monks, P. S., and Ellis, A. M.: Proton-transfer reaction mass spectrometry, Chem. Rev., 109, 861–896, 2009.

Blake, R. S., Wyche, K. P., Ellis, A. M., and Monks, P. S.: Chemical ionization reaction time-of-flight mass spectrometry: Multi-reagent analysis for determination of trace gas composition, Int. J. Mass Spectrom., 254, 85–93, 2006.

Blake, R. S., Whyte, C., Hughes, C. O., Ellis, A. M., and Monks, P. S.: Demonstration of proton-transfer reaction time-of-flight mass spectrometry for real-time analysis of trace volatile organic compounds, Anal. Chem., 76, 3841–3845, 2004.

Bonn, B. and Moortgat, K.: Sesquiterpene ozonolysis: Origin of atmospheric new particle formation from biogenic hydrocarbons, Geophys. Res. Lett., 30, 1585, doi:10.1029/2003GL017000, 2003.

Bouvier-Brown, R. C., Holzinger, R., Palitzsch, K., and Goldstein, H.: Large emissions of sesquiterpenes and methyl chavicol quantified from branch enclosure measurements, Atmos. Environ., 43, 389–401, 2009.

Boy, M., Karl, T., Turnipseed, A., Mauldin, R. L., Kosciuch, E., Greenberg, J., Rathbone, J., Smith, J., Held, A., Barsanti, K., Wehner, B., Bauer, S., Wiedensohler, A., Bonn, B., Kulmala, M., and Guenther, A.: New particle formation in the Front Range of the Colorado Rocky Mountains, Atmos. Chem. Phys., 8, 1577–1590, doi:10.5194/acp-8-1577-2008, 2008.

Canosa-Mas, C. E., King, M. D., Scarr, P. J., Thompson, K. C., and Wayne, R. P.: An experimental study of the gas-phase reactions of the NO_3 radical with three sesquiterpenes:

isolongifolene, alloisolongifolene, and [small alpha]-neoclovene, Phys. Chem. Chem. Phys., 1, 2929–2933, 1999.

Demarcke, M., Amelynck, C., Schoon, N., Dhooghe, F., Van Langenhove, H., and Dewulf, J.: Laboratory studies in support of the detection of sesquiterpenes by proton-transfer-reaction-mass-spectrometry, Int. J. Mass Spectrom., 279, 156–162, 2009.

Dhooghe, F., Amelynck, C., Schoon, N., Debie, E., Bultinck, P., and Vanhaecke, F.: A selected ion flow tube study of the reactions of H_3O^+, NO^+ and O_2^+ with a series of sesquiterpenes, Int. J. Mass Spectrom., 272, 137–148, 2008.

Duhl, T. R., Helmig, D., and Guenther, A.: Sesquiterpene emissions from vegetation: a review, Biogeosciences, 5, 761–777, doi:10.5194/bg-5-761-2008, 2008.

Ezra, D., Jasper, J., Rogers, T., Knighton, B., Grimsrud, E., and Strobel, G.: Proton transfer reaction-mass spectrometry as a technique to measure volatile emissions of Muscodor albus, Plant Sci., 166, 1471–1477, 2004.

Helmig, D. and Arey, J.: Organic chemicals in the air at Whitaker's Forest/Sierra Nevada Mountains, California, Sci. Total Environ., 112, 233–250, 1992.

Helmig, D., Revermann, T., Pollmann, J., Kaltschmidt, O., Jiménez Hernández, A., Bocquet, F., and David, D.: Calibration system and analytical considerations for quantitative sesquiterpene measurements in air, J. Chromatogr. A, 1002, 193–211, 2003.

De Hoffmann, E. and Stroobant, V.: Mass spectrometry – Principles and applications, 3rd Edn., John Wiley & Sons, 489 pp., 2007.

Holopainen, J. K. and Gershenzon, J.: Multiple stress factors and the emission of plant VOCs, Trends Plant Sci., 15, 176–184, 2010.

Ibrahim, Y. M., Prior, D. C., Baker, E. S., Smith, R. D., and Belov, M. E.: Characterization of an ion mobility-multiplexed collision-induced dissociation-tandem time-of-flight mass spectrometry approach, Int. J. Mass Spectrom., 293, 34–44, 2010.

Jordan, A., Haidacher, S., Hanel, G., Hartungen, E., Herbig, J., Märk, L., Schottkowsky, R., Seehauser, H., Sulzer, P., and Märk, T. D.: An online ultra-high sensitivity proton-transfer-reaction mass-spectrometer combined with switchable reagent ion capability (PTR+SRI-MS), Int. J. Mass Spectrom., 286, 32–38, 2009.

Jordan, A., Haidacher, S., Hanel, G., Hartungen, E., Märk, L., Seehauser, H., Schottkowsky, R., Sulzer, P., and Märk, T. D.: A high resolution and high sensitivity time-of-flight proton-transfer-reaction mass spectrometer (PTR-TOF-MS), Int. J. Mass Spectrom., 286, 122–128, 2009.

Kesselmeier, J. and Staudt, M.: Biogenic Volatile Organic Compounds (VOC): an overview on

emission, physiology and ecology, J. Atmos. Chem., 33, 23–88, 1999.

Kim, S., Karl, T., Helmig, D., Daly, R., Rasmussen, R., and Guenther, A.: Measurement of atmospheric sesquiterpenes by proton transfer reaction-mass spectrometry (PTR-MS), Atmos. Meas. Tech., 2, 99–112, doi:10.5194/amt-2-99-2009, 2009.

Knighton, B., Fortner, E. C., Herndon, S. C., Wood, E. C., and Miake-Lye, R. C.: Adaptation of a proton transfer reaction mass spectrometer instrument to employ NO^+ as reagent ion for the detection of 1,3-butadiene in the ambient atmosphere, Rapid Commun. Mass Sp., 23, 3301–3308, 2009.

Lee, A., Goldstein, A. H., Keywood, M. D., Gao, S., Varutbangkul, V., Bahreini, R., Ng, N. L., Flagan, R. C., and Seinfeld, J. H.: Gas-phase products and secondary aerosol yields from the ozonolysis of 16 different terpenes, J. Geophys. Res., D17305, doi:10.1029/2005JD006437, 2006a.

Lee, A., Goldstein, A. H., Keywood, M. D., Gao, S., Varutbangkul, V., Bahreini, R., Ng, N. L., Flagan, R. C., and Seinfeld, J. H.: Gas-phase products and secondary aerosol yields from the ozonolysis of ten different terpenes, J. Geophys. Res., D07302, doi:10.1029/2005JD006437, 2006b.

Loreto, F. and Schnitzler, J.-P.: Abiotic stresses and induced BVOCs, Trends Plant Sci., 15, 154–166, 2010.

Müller, M., Mielke, L. H., Breitenlechner, M., McLuckey, S. A., Shepson, P. B., Wisthaler, A., and Hansel, A.: MS/MS studies for the selective detection of isomeric biogenic VOCs using a Townsend Discharge Triple Quadrupole Tandem MS and a PTR-Linear Ion Trap MS, Atmos. Meas. Tech., 2, 703–712, doi:10.5194/amt-2-703-2009, 2009.

Muntean, F. and Armentrout, P. B.: Guided ion beam study of collision-induced dissociation dynamics: integral and differential cross sections, J. Chem. Phys., 115, 1213–1228, 2001.

Novak, I., Kovac, B., and Kovacevic, G.: Electronic structure of terpenoids, J. Org. Chem., 66, 4728–4731, 2001.

Paré, P. W. and Tumlinson, J. H.: De novo biosynthesis of volatiles induced by insect herbivory in cotton plants, Plant Physiol., 114, 1161–1167, 1997.

Paré, P. W. and Tumlinson, J. H.: Plant volatiles as a defense against insect herbivores, Plant Physiol., 121, 135–331, 1999.

Peñuelas, J. and Staudt, M.: BVOCs and global change, Trends Plant Sci., 15, 133–144, 2010.

Pichersky, E. and Gershenzon, J.: The formation and function of plant volatiles: perfumes for pollinator attraction and defense, Curr. Opin. Plant Biol., 5, 237–243, 2002.

Rimetz-Planchon, J., Schoon, N., Amelynck, C., and Dhooghes, F.: Collision induced dissociation in a flowing afterglow-tandem mass spectrometer for the selective detection of C5 unsaturated alcohols and isoprene, Int. J. Mass Spectrom., 289, 30–38, 2010.

Smith, D. and Španĕl, P.: Selected ion flow tube mass spectrometry (SIFT-MS) for on-line trace gas analysis, Mass Spectrom. Rev., 24, 661–700, 2005.

Španĕl, P., Ji, Y., and Smith, D.: SIFT studies of the reactions of H_3O^+, NO^+ and O_2^+ with a series of aldehydes and ketones, Int. J. Mass Spectrom., 165–166, 25–37, 1997.

Španĕl, P. and Smith, D.: SIFT studies of the reactions of H_3O^+, NO^+ and O_2^+ with a series of alcohols, Int. J. Mass Spectrom., 167–168, 375–388, 1997

Španĕl, P. and Smith, D.: Selected ion flow tube studies of the reactions of H_3O^+, NO^+, and O_2^+ with several aromatic and aliphatic hydrocarbons, Int. J. Mass Spectrom., 181, 1–10, 1998.

Thomson, B. A., Douglas, D. J., Corr, J. J., Hager, J. W., and Jolliffe, C. L.: Improved collisionally activated dissociation efficiency and mass resolution on a triple quadrupole mass spectrometer system, Anal. Chem., 67, 1696–1704, 1995.

Wyche, K. P., Blake, R. S., Willis, K. A., Monks, P. S., and Ellis, A. M.: Differentiation of isobaric compounds using chemical ionization reaction mass spectrometry, Rapid Commun. Mass Sp., 19, 3356–3362, 2005.

Yost, R. A., Enke, C. G., McGilvery, D. C., Smith, D., and Morrison, J. D., High efficiency collision-induced dissociation in an RF-only quadrupole, Int. J. Mass Spectrom., 30, 127–136, 1979.

Table 1. Families of fragments from the fragmentation of *m/z* 205 and *m/z* 204. In bold: fragment ions with a maximum fragmentation fraction >10%. For the fragmentation of ions at *m/z* 204, EE^+ and $OE^{\bullet+}$ fragments are distinguished. ◇ observed by Dooghe et al. (2008); □ observed by Demarcke et al. (2009); ∗ observed by Lee et al. (2006a); ▲ observed by Kim et al. (2009); and ● observed by Ezra et al. (2004).

Fragmentation of protonated SQT (*m/z* 205)											
A		B		C		D		E			
								29	$C_2H_5^+$		
						41	$C_3H_5^+$	43	$C_3H_7^+$		
						55	$C_4H_7^+$	57*	$C_4H_9^+$		
				67*	$C_5H_7^+$	**69**	$C_5H_9^+$	71*	$C_5H_{11}^+$		
77	$C_6H_5^+$	79	$C_6H_7^+$	**81**$^{\diamond,\square,\ast,\blacktriangle,\bullet}$	$C_6H_9^+$	**83***	$C_6H_{11}^+$	85*	$C_6H_{13}^+$		
91	$C_7H_7^+$	**93**$^{\square,\bullet}$	$C_7H_9^+$	**95**$^{\diamond,\square,\ast,\blacktriangle}$	$C_7H_{11}^+$	97*	$C_7H_{13}^+$				
105	$C_8H_9^+$	**107**$^{\square}$	$C_8H_{11}^+$	**109**$^{\diamond,\square,\ast,\blacktriangle,\bullet}$	$C_8H_{13}^+$	111	$C_8H_{15}^+$				
119	$C_9H_{11}^+$	**121**$^{\diamond,\square,\ast}$	$C_9H_{13}^+$	**123**$^{\diamond,\square,\ast,\blacktriangle,\bullet}$	$C_9H_{15}^+$	125*	$C_9H_{17}^+$				
133*	$C_{10}H_{13}^+$	**135**$^{\diamond,\square,\ast,\blacktriangle,\bullet}$	$C_{10}H_{15}^+$	137$^{\diamond,\square,\ast\blacktriangle}$	$C_{10}H_{17}^+$						
147*	$C_{11}H_{15}^+$	**149**$^{\diamond,\square,\ast,\blacktriangle,\bullet}$	$C_{11}H_{17}^+$								
161	$C_{12}H_{17}^+$	**163**$^{\square,\ast}$	$C_{12}H_{19}^+$								
		177*	$C_{13}H_{21}^+$								
Fragmentation of SQT molecular ions (*m/z* 204) – EE^+ fragments											
A		B		C		D		E		F	
								29	$C_2H_5^+$		
						41	$C_3H_5^+$	43	$C_3H_7^+$		
						55	$C_4H_7^+$	57	$C_4H_9^+$		
		65	$C_5H_5^+$	67	$C_5H_7^+$	69	$C_5H_9^+$	71	$C_5H_{11}^+$		
77	$C_6H_5^+$	79	$C_6H_7^+$	81	$C_6H_9^+$	83	$C_6H_{11}^+$	85	$C_6H_{13}^+$		
91	$C_7H_7^+$	93	$C_7H_9^+$	95	$C_7H_{11}^+$	97	$C_7H_{13}^+$				
105	$C_8H_9^+$	107	$C_8H_{11}^+$	109	$C_8H_{13}^+$	111	$C_8H_{15}^+$				
119	$C_9H_{11}^+$	**121**	$C_9H_{13}^+$	123	$C_9H_{15}^+$						
133	$C_{10}H_{13}^+$	135	$C_{10}H_{15}^+$	137	$C_{10}H_{17}^+$					131	$C_{10}H_{11}^+$
147$^{\diamond}$	$C_{11}H_{15}^+$	149	$C_{11}H_{17}^+$							145	$C_{11}H_{13}^+$
161$^{\diamond}$	$C_{12}H_{17}^+$										
175	$C_{13}H_{19}^+$										
189$^{\diamond}$	$C_{14}H_{21}^+$										
Fragmentation of SQT molecular ions (*m/z* 204) – $OE^{\bullet+}$ fragments											
a		b		c		d		e			
								42	$C_3H_6^{\bullet+}$		
								56	$C_4H_8^{\bullet+}$		
								70	$C_5H_{10}^{\bullet+}$		
				80$^{\diamond}$	$C_6H_8^{\bullet+}$	82	$C_6H_{10}^{\bullet+}$	98	$C_7H_{14}^{\bullet+}$		
		92	$C_7H_8^{\bullet+}$	**94**	$C_7H_{10}^{\bullet+}$	96	$C_7H_{12}^{\bullet+}$				
		106	$C_8H_{10}^{\bullet+}$	**108**	$C_8H_{12}^{\bullet+}$	110	$C_8H_{14}^{\bullet+}$				
118	$C_9H_{10}^{\bullet+}$	**120**	$C_9H_{12}^{\bullet+}$	**122**	$C_9H_{14}^{\bullet+}$						
		134$^{\diamond}$	$C_{10}H_{14}^{\bullet+}$	136	$C_{10}H_{16}^{\bullet+}$						
		148$^{\diamond}$	$C_{11}H_{16}^{\bullet+}$								
		162$^{\diamond}$	$C_{12}H_{18}^{\bullet+}$								
		176$^{\diamond}$	$C_{13}H_{20}^{\bullet+}$								

Table 2. Fragment ions from the fragmentation of SQT molecular ions (*m/z* 204). In bold, NO^+/SQT product ions observed in SIFT-MS (Dhooghe et al., 2008). MFF = Maximum Fragmentation Fraction; FF = Fragmentation Fraction at 0.68 eV. E_{CM} (eV) indicates the range of E_{CM} where MFF is found.

SQT	*m/z*	MFF	E_{CM} (eV)	FF at 0.68 eV
α-Humulene	105	40	>6	
	122	10	<2	
	147	58	<2	52
	161	11	<3	11
Aromadendrene	94	10	<2	
	105	11	>6	
	119	13	>6	
	133	19	<2	
	161	31	<3	31
	189	12	<3	
α-Cedrene	105	14	>6	
	108	16	<2	16
	119	37	>3	25
	147	15	<2	15
	161	19	<2	
Longifolene	119	12	>6	
	133	17	>3	
	161	72	<2	37
	189	17	<2	17
δ-Neoclovene	105	11	>6	
	119	18	>6	
	120	12	1.5–3.5	
	121	13	>4	
	161	12	<3	
	162	80	<2	71
Isolongifolene	119	12	>6	
	133	15	>6	
	147	25	<3	24
	161	66	<3	66
β-Caryophyllene	105	11	>6	
	133	20	>3	
	147	14	<1	14
	148	12	<1	
	161	37	<2	32
	175	10	<1	
	189	17	<2	16

Table 3. Fragment ions with maximum fragmentation fraction >10% from the fragmentation of CI fragment ions from the reaction between β-caryophyllene and NO^+.

Parent *m/z*	Fragments *m/z*	MFF (%)	E_{CM} (eV)	Parent *m/z*	Fragments *m/z*	MFF (%)	E_{CM} (eV)
148	133	38	3	176	161	37	>4
	119	11	4		134	14	>4
	106	24	3		133	12	>4
	105	15	>5		120	14	>4
	91	26	6		119	20	>4
					105	16	>4
161	133	11	3	189	147	11	4
	119	23	4		133	19	4
	105	32	4		119	14	4
	91	16	>6		105	12	>6
	81	11	4		95	15	4

Table 4. Fragmentation fractions of tracers for δ-neoclovene, α-cedrene, longifolene and α-humulene based on the fragmentation of the molecular ions at *m/z* 204. N.O.: peaks not observed under our experimental conditions. Note that results are not corrected for mass discrimination effects.

SQT	*m/z* 162–0.68 eV	*m/z* 119–0.68 eV	*m/z* 131–0.68 eV	*m/z* 137–2.5 eV	*m/z* 83–6.1 eV	%PID *m/z* 204[1]
Aromadendrene	3.9 ± 0.2	2.4 ± 0.2	N.O.	N.O.	0.49 ± 0.05	94
α-cedrene	N.O.	**24.5 ± 0.8**	0.24 ± 0.04	N.O.	0.40 ± 0.03	98
longifolene	N.O.	0.57 ± 0.04	N.O.	**4.9 ± 0.1**	N.O.	93
δ-neoclovene	**71 ± 1**	0.97 ± 0.05	N.O.	N.O.	**9.3 ± 0.2**	94
isolongifolene	N.O.	1.3 ± 0.2	N.O.	N.O.	0.44 ± 0.04	99
α-humulene	0.96 ± 0.08	1.7 ± 0.1	**3.8 ± 0.2**	N.O.	0.17 ± 0.02	77
β-caryophyllene	N.O.	0.47 ± 0.05	N.O.	N.O.	0.33 ± 0.03	59

[1] Data obtained by SIFT-MS (Dhooghe et al., 2008)

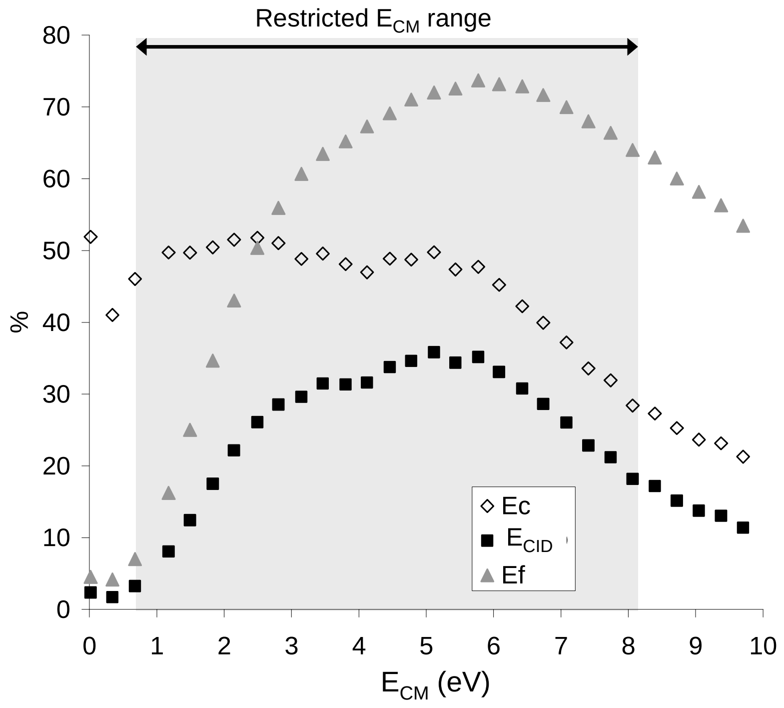

Fig. 1. Collection (E_c), fragmentation (E_f) and CID (E_{CID}) efficiencies (in %) as a function of collision energy (E_{CM}) for the fragmentation of protonated α-cedrene. The restricted E_{CM} range considered in this study is indicated.

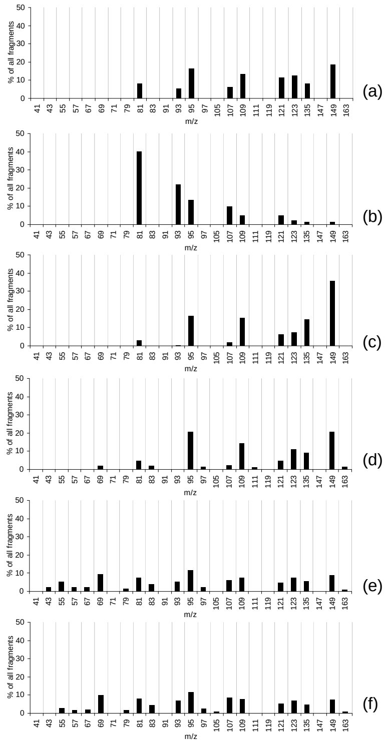

Fig. 2. Fragmentation patterns of protonated α-humulene obtained by **(a–c)** Müller et al. (2009) (QqQ-MS and PTR-LIT) and by **(d–f)** FA-TMS at three different E_{CM}. For FA-TMS, only fragments >1% are shown. **(a)** $U_{\mathrm{cc}} = 12\,\mathrm{V}$, **(b)** $U_{\mathrm{cc}} = 33\,\mathrm{V}$, **(c)** $U_{\mathrm{CID,PTR\text{-}LIT}} = 0.13\,\mathrm{V}$, **(d)** $E_{\mathrm{CM}} = 0.68\,\mathrm{eV}$, **(e)** $E_{\mathrm{CM}} = 5.1\,\mathrm{eV}$, and **(f)** $E_{\mathrm{CM}} = 6.4\,\mathrm{eV}$.

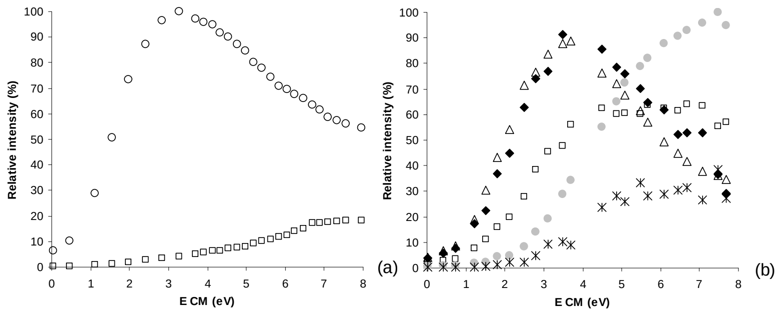

Fig. 3. Fragmentation patterns of **(a)** *m/z* 147 from α-humulene and **(b)** *m/z* 162 from δ-neoclovene as a function of collision energy. (○) *m/z* 105, (△) *m/z* 147, (●) *m/z* 91, (⚹) *m/z* 105, (◆) *m/z* 106 and (□) other fragment ions. Experimental error, not indicated on the graph for more clarity, varies between 0.5 and 29%.

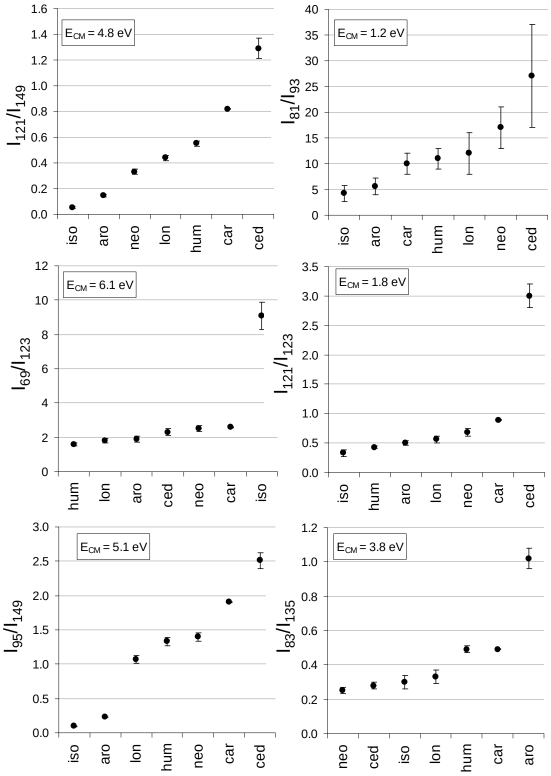

Fig. 4. Selected fragment ion intensity ratios from the fragmentation of protonated SQT. Error bars correspond to 2σ.